

Aqueous Synthesis of Tailored ZnO Nanocrystals, Nanocrystal Assemblies, and Nanostructured Films by Physical Means Enabled by a Continuous Flow Microreactor

The Faculty of Oregon State University has made this article openly available.
Please share how this access benefits you. Your story matters.

Citation	Choi, C. H., & Chang, C. H. (2014). Aqueous Synthesis of Tailored ZnO Nanocrystals, Nanocrystal Assemblies, and Nanostructured Films by Physical Means Enabled by a Continuous Flow Microreactor. <i>Crystal Growth & Design</i> , 14 (9), 4759-4767. doi:10.1021/cg500911w
DOI	10.1021/cg500911w
Publisher	American Chemical Society
Version	Accepted Manuscript
Terms of Use	http://cdss.library.oregonstate.edu/sa-termsfuse

1 Aqueous Synthesis of Tailored ZnO Nanocrystals,
2 Nanocrystal Assemblies, and Nanostructured Films
3 by Physical Means Enabled by a Continuous Flow
4 Microreactor

5 *Chang-Ho Choi and Chih-hung Chang**

6 Oregon Process Innovation Center/ Microproduct Breakthrough Institute and School of
7 Chemical, Biological & Environmental Engineering, Oregon State University, Corvallis, OR
8 97331, United States

9 KEYWORDS: Solution-based process, Microreactor, Nanocrystal assembly, Zinc oxide film

10 ABSTRACT. ZnO nanofilms with four distinctly different morphologies were fabricated by
11 adjusting physical parameters including the flow rate of the solution and RPM of the rotating
12 disk in the continuous flow microreactor system while keeping the same chemical precursors,
13 precursor solution concentration, and reaction temperature. Controlled reactive species including
14 colloidal ZnO nanocrystal, ZnO assemblies, molecular and ionic precursors were synthesized
15 from a microreactor at 70 °C reaction temperature by changing flow rate of the solution. These
16 reactive species were directly delivered onto a thermally grown oxide layer (100 nm) of Si
17 substrate (1.5 cm × 1.5 cm) at 80 °C deposition temperature to densely form a flower-like film,

1 amorphous film, vertical nanowire (NW) arrays, and crystalline film. ZnO assemblies were
2 delivered onto the substrate and served as seed layers to form flower-like film. Amorphous film
3 were formed after depositing Zn(OH)_3^- ionic species on the substrate. For the vertical ZnO NW
4 arrays colloidal ZnO nanoparticles, delivered onto the amorphous layer, formed a polycrystalline
5 ZnO layer and NWs were grown subsequently after Zn(OH)_3^- deposition onto the polycrystalline
6 ZnO layer. Lastly, crystalline film was fabricated by delivering ZnO assemblies onto the
7 amorphous layer followed by Zn(OH)_3^- deposition. Thickness and size of all the films were
8 found to be varied by deposition period. In contrast, only powdery flower-like ZnO could be
9 obtained using a batch reactor at the same reaction conditions. ZnO nanofilms were also
10 deposited on stainless steel substrate (SS304) for the two-phase pool boiling experiment to
11 investigate structural impact of the nanofilms on boiling heat transfer performances. The boiling
12 performance was significantly impacted by the structure of the nanofilms. The highest boiling
13 performance was achieved by the crystalline film, exhibiting a heat transfer coefficient of 4.2
14 $\text{W/cm}^2 \text{ K}$ along with a critical heat flux of about 100 W/cm^2 . This work demonstrates a highly-
15 controlled and scalable process for the fabrication of tailored metal oxide nanofilms.

16

1 INTRODUCTION

2 Nanostructured metal oxides are playing important roles in many applications including energy
3 generation and storage¹, environmental, electronic, chemical and biological systems.^{2, 3} ZnO is
4 probably the most studied material among various metal oxides due to its wide, direct bandgap,
5 wide variety of nanostructure shapes, easier crystal growth techniques, and earth abundance.⁴⁻⁸
6 Significant efforts in synthetic methodologies via both gas-phase^{9, 10} and solution-phase routes¹¹⁻
7 ¹³ have been made to control phase and morphology of ZnO.^{14, 15} Gas phase synthesis methods
8 such as vapor phase transport, physical vapor deposition and metal organic chemical vapor
9 deposition are normally carried out at high temperatures using higher cost capital equipment.
10 Solution-phase methods including chemical bath deposition, hydrothermal, and sol-gel offer
11 lower temperature routes for the synthesis of ZnO nanostructures. In solution-phase approaches,
12 solution conditions such as pH value, precursors including reactants and surfactants, reaction
13 temperature, and concentration of precursor are commonly used to control ZnO morphologies.
14 Continuous flow microreactors offer several advantages for the synthesis of ZnO nanostructures.
15 The primary advantage of microreactors is to generate homogeneous reaction circumstances by
16 minimizing the gradient of the reaction temperature and precursor concentration, leading to
17 monodisperse nanoparticles formation. A few studies have been reported concerning the
18 application of microreactors to the synthesis of ZnO nanostructures. Han *et al.* fabricated
19 transparent nanocrystalline ZnO thin film transistors using a continuous-flow microreactor.¹⁶
20 Jung *et al.* deposited flower-like ZnO structures with different morphologies by changing
21 temperature and NaOH concentration of the solution.¹⁷ Li *et al.* used micro continuous-flow
22 process to synthesize spherical, cylinder-, star- and flower-like ZnO microparticles.¹⁸ Different
23 morphologies were obtained in the microreactor by changing the precursor concentration and pH.

1 Mc Peak and Baxter deposited vertical ZnO nanowire (NW) arrays by flowing chemical solution
2 through a submillimeter channel. Substrates (Si and soda lime glass) were seeded with a thin ZnO
3 film by dip coating before NW deposition. Spatially resolved characterizations reveal that the
4 NW length decreased, morphology changed along the direction of flow.^{19,20} Most recently, Han
5 *et al.* reported a high-rate deposition of a nanostructured ZnO anti-reflective coating on a
6 textured silicon substrate seeded with Ag nanoparticles using a table-top, microreactor-assisted
7 solution deposition process.²¹

8 Here, we demonstrate controlling ZnO nanofilm morphology simply by varying the physical
9 process parameters while using identical chemical precursors via a solution-route without adding
10 surfactants for the first time. The prepared ZnO films include a flower-like nanofilm, amorphous
11 nanofilm, vertical NW arrays, and crystalline nanofilm. These films were fabricated using a
12 continuous flow microreactor and deposition system. ZnO nanocrystal assemblies of different
13 structures were synthesized by controlling the solution flow rate.^{22, 23} These nanocrystal
14 assemblies, which were made *in-situ* in the microreactor, were delivered directly onto a substrate
15 to be the seed layer for the first time. The molecular and ionic precursors, Zn(OH)_2 (aq),
16 Zn(OH)_3^- and Zn(OH)_4^{2-} , were subsequently deposited onto the seed layer to form various ZnO
17 nanofilms. This work shows the feasibility to grow distinctly different ZnO nanostructured thin
18 films simply by physical means (i.e. the flow rate of the solution and the rotating speed of the
19 substrate). All nanostructured films of different morphologies reported in this work were grown
20 using exactly the same precursors, same concentration and same solution temperature. This is
21 accomplished by using a microreactor to create a reacting chemical solution with different
22 building blocks (including different ZnO seeds generated *in-situ*) via homogeneous reaction in
23 the solution then deliver the solution to the substrate surface to achieve controlled heterogeneous

1 film growth. This work adds another dimension to control the ZnO nanostructured film
2 morphologies other than chemical means (e.g. adding surfactants, varying pH, different counter
3 ions).

4 The impact of different micro- and nanostructures of these ZnO nanofilms was demonstrated via
5 two-phase pool boiling experiments using these nanofilms as the boiling surfaces.

6

7 EXPERIMENTAL APPROACH

8 **Fabrication of ZnO nanofilms:** The deposition system to prepare ZnO nanocrystals consists
9 of a microprocessor controlled dispensing pump (Ismatec), Tygon tubing (1.22 mm ID,
10 Upchurch Scientific), and a micro T-mixer (Upchurch scientific). The micro T-mixer is made by
11 polyether ether ketone (PEEKTM) material, and diameter of the channel inside the mixer is about
12 50 μm . The mixer has two inlet streams and one outlet stream. Zinc acetate
13 ($\text{Zn}(\text{CH}_3\text{COO})_2 \cdot 6\text{H}_2\text{O}$, Sigma Aldrich), ammonium acetate ($\text{CH}_3\text{COONH}_4$, Mallinckrodt
14 Chemicals), and sodium hydroxide (NaOH, Mallinckrodt Chemicals) were used as received
15 without further purification. Stream A (0.005 M $\text{Zn}(\text{CH}_3\text{COO})_2 \cdot 6\text{H}_2\text{O}$ and 0.025 M
16 $\text{CH}_3\text{COONH}_4$ solution) and stream B (0.1 M NaOH) were dissolved in de-ionized (D.I.) water
17 and initially pumped into the mixer. The micro-T-mixer allowed the homogeneous mixing of the
18 reactants. Then, the mixture of the reactants passed through a helical reactor made by wrapping
19 1.3 m long Tygon tubing around a cylinder. By immersing the reactor in a water bath, the
20 reaction temperature (70 $^\circ\text{C}$) was maintained throughout the growth process. Three different
21 volume flow rates (6.8, 14.7, and 28.1 mL min^{-1}) were employed to form the ZnO assemblies.
22 All of chemical reagents including molecular precursors, individual nanocrystals, and the
23 assemblies were directly deposited onto a 1.5 cm \times 1.5 cm thermally grown oxide layer of Si

1 substrate sitting on the temperature controllable rotating disk. Approximately 100 nm thick oxide
2 layer was grown on Si substrate through thermal annealing process at 1000 °C for three hours.
3 RPM of the rotating disk was varied, and the deposition temperature was fixed approximately to
4 80°C during the deposition process. The SiO₂ substrate was vigorously cleaned by using acetone,
5 methanol, and deionized water followed by the drying with nitrogen gas. The substrate was then
6 treated with O₂ plasma for the enhanced adherence of the chemical reagents. O₂ plasma surface
7 treatment was performed by using a bench top plasma cleaner (Plasma Etch, PE-50 XL) with
8 operation conditions of 50 W power and a four minute treatment period. The ZnO on the
9 substrate was washed with D.I. water and sonicated.

10 For the ZnO growth in the batch process, same concentration of precursor and same reaction
11 temperature applied to the continuous flow microreactor were used. The pH value of mixed
12 solution was measured to be around 11.3. The aqueous solution including zinc acetate and
13 ammonium acetate was mixed with aqueous sodium hydroxide solution in a beaker. The
14 substrate was placed inside the beaker, and the beaker was placed in the oven maintained at 70
15 °C. After 30 minute reaction time, the solution became turbid. Both ZnO powder in the solution
16 and ZnO on the substrate were collected after two hour reaction period. The ZnO on the substrate
17 was washed with D.I. water and sonicated.

18 **Characterization of ZnO nanocrystals and nanofilms:** Size and morphology of colloidal
19 ZnO nanocrystals and assembly were analyzed using high resolution transmission electron
20 microscopy (HRTEM) and fast fourier transform (FFT). HRTEM images were taken by using a
21 FEI Titan operated at 300 kV. For the HRTEM analysis, ZnO nanocrystals generated inside the
22 helical reactor were directly delivered on a carbon coated copper grid (300 mesh, Tedpella).
23 Several approaches of collecting ZnO nanocrystals on grids were tested to verify that the

1 observed ZnO assembly under TEM is independent of TEM sample preparation method. We
2 observed that evaporation of solvent did not affect assemblies of ZnO nanocrystals. For the
3 HRTEM analysis of the amorphous film, a focused ion beam (FIB) technique was performed.
4 Platinum (Pt) layer was deposited on the top of the ZnO layer to protect the ZnO layer during the
5 FIB process. Morphologies of the nanofilms were examined by scanning electron microscopy
6 (SEM, Quanta 600 FEG) and atomic force microscopy (AFM, Veeco). X-ray diffraction (XRD)
7 was used to identify the crystallinity of the nanofilms. XRD data was obtained by using D8
8 Discover (Bruker) with Cu K α radiation (acceleration voltage: 40 kV, flux: 40 mA). UV-visible
9 spectrum (Ocean Optics) was taken to analyze the optical band gap of the nanofilms. For the
10 optical band gap measurement, four distinct ZnO films were deposited on micro slide glass
11 substrates. The Davis-Mott and Tauc models were employed to estimate the optical band gap of
12 the films²⁴.

13 **Pool boiling experiments:** All of the ZnO thin films for pool boiling experiments were
14 deposited on the 1" \times 1" stainless steel substrate (SS 304). Procedures to prepare ZnO nanofilms
15 on SS304 substrates were identical to the procedures for the growth of ZnO nanofilms on SiO₂/Si
16 substrates. Boiling surfaces were characterized by the contact angle measurement with a static
17 sessile drop method (FTA 137). The average static contact angle was estimated by dropping 2
18 μ L D.I. water on the five different areas of the films. The shape of the droplet was captured using
19 a high speed camera, and the contact angle was estimated from the captured image. The boiling
20 experimental set-up and experimental procedures can be found in our previous report [25].

21

22 RESULTS AND DISCUSSION

1 We have recently demonstrated that the effect of external convective forces generated from a
2 fluid flow in a winding capillary tube can lead to unique assemblies of colloidal ZnO
3 nanocrystals from an aqueous solution.²³ The molecular precursors as a function of pH values are
4 shown according to the speciation diagram (Figure 1). The solution acidity required to grow
5 colloidal ZnO nanocrystals was measured to be around pH=12.5. At pH=12.5, Zn(OH)_3^- is the
6 dominant species along with Zn(OH)_4^{2-} and Zn(OH)_2 (aq). HRTEM images of colloidal ZnO
7 nanocrystals and their assemblies synthesized by the continuous flow microreactor at different
8 flow rates are shown in Figure 2. At a low flow rate of 6.8 mL min^{-1} , individual colloidal ZnO
9 nanocrystals were grown and dispersed in the solution without forming assembly (Figure 2a). On
10 the other hand, at a higher flow rate (14.7 mL min^{-1}) colloidal ZnO nanocrystals aggregated,
11 forming rectangular assembly structures with various lengths and widths (Figure 2b). The
12 structure, consisting of a number of ZnO nanocrystals, was formed by random aggregation of
13 individual ZnO nanocrystals exhibiting polycrystalline, as confirmed by a closer view of the
14 structure and the corresponding FFT image. At this flow rate, the effect of Dean vortices is
15 significant and competes with electrostatic forces.^{22, 23} This competing interaction resulted in the
16 formation of the rectangular ZnO assembly. At a flow rate of 28.1 mL min^{-1} , large spherical
17 assemblies composed of colloidal ZnO nanocrystals with a surrounding amorphous ZnO matrix
18 were formed (Figure 2c and 2d). The reactive chemical flux including Zn(OH)_3^- , Zn(OH)_2 (aq),
19 and Zn(OH)_4^{2-} , individual colloidal ZnO nanocrystals along with their assemblies were directly
20 delivered onto a substrate to fabricate ZnO nanofilms. ZnO nanofilms completely cover entire
21 areas of the substrate except for some edge areas taped to secure the substrate on the rotating
22 disk during the deposition process.

1 Using the solution generating from the microreactor with a flow rate of 14.7 and 28.1 mL min⁻¹
2 ¹, deposition experiments were performed at 0 RPM of the rotating disk for a three minute
3 deposition period. Both experiments produced flower-like ZnO film as displayed in Figure 3a
4 and 3b. Interestingly, the flower-like ZnO crystals show different morphologies. The flower-like
5 structures formed at 14.7 mL min⁻¹ are generally larger than those formed at 28.1 mL min⁻¹. In
6 addition, the flower-like structures formed at higher flow rate appear to have more petals. Under
7 the condition of 0 RPM of the rotating disk, the assemblies can stay on the surface and serve as
8 seeds, and the molecular precursors were subsequently deposited on the seeds to form the
9 flower-like ZnO structure on the surface. We believe the difference in morphology of these two
10 flower-like structures is a result of different seeds from the microreactor. The XRD pattern of
11 both flower-like structures matches well with the pattern of pure Wurtzite structure (JCPDS Card
12 No. 36-1451) (Figure 3e). A typical flower-like structure was analyzed using HRTEM (Figure
13 3f). The periphery of the flower-like structure shows single crystallinity, indicating that the petal
14 began to grow from the basal plane.²⁶

15 Surprisingly, amorphous ZnO nanofilms were obtained using a solution with a flow rate of
16 28.1 mL min⁻¹ and 1500 RPM of the rotating disk. The amorphous film is very smooth and
17 uniform as shown by the SEM image and AFM image given in Figure 4a and 4b. The average
18 roughness of the film was measured to be around 0.34 nm. The film with a thickness around 15
19 nm can be obtained from a three minute deposition period as displayed in the HRTEM image
20 (Figure 4c). The amorphous phase of the film was confirmed by a FFT image and XRD pattern
21 (Figure 4c and 4d). At a flow rate of 28.1 mL min⁻¹, the solution from the helical reactor includes
22 a mixture of molecular precursors, individual nanocrystals, and spherical assemblies formed by
23 the aggregation of nanocrystals. If the assemblies or individual nanocrystals served as the

1 building blocks or seed layers for the film formation, nanocrystalline ZnO thin film should be
2 obtained. We replaced the helical reactor with a short linear reactor that only generates the
3 molecular precursors. Smooth, amorphous thin films were also obtained. This experiment clearly
4 demonstrates that the spherical assemblies are not associated with the amorphous film formation.
5 Therefore, we believe that molecular precursors are the primary building blocks for the
6 formation of amorphous ZnO films. The rotation motion of the substrate significantly reduces the
7 probability of ZnO nanocrystals and their assemblies to stick on the surface as seeds. A series of
8 high and low resolution SEM images of flower-like structures formed at different RPM are given
9 in Figure 5. These images clearly show a reduction of density of flower-like structures at a
10 higher RPM and reduced size of the flower-like structures compared to those at 0 RPM.

11 Vertical ZnO NW arrays have been intensively researched over the last decade in wide variety
12 of applications.²⁷⁻³¹ Researchers have reported various seed layers for the growth of vertical ZnO
13 NW arrays, including ZnO nanocrystals³²⁻³⁴ and metallic nanocrystals.³⁵ On our amorphous ZnO
14 surface, vertical ZnO NW arrays can also be fabricated from the same starting precursors with
15 the same concentration at the same temperature. It was found that we cannot produce the vertical
16 ZnO NW arrays in the absence of the amorphous layer. To fabricate vertical ZnO NW arrays, we
17 first deposited an amorphous ZnO layer on the SiO₂/Si substrate. Vertical ZnO NW arrays on the
18 amorphous ZnO surface were then fabricated using a 6.8 mL min⁻¹ flow rate solution on
19 substrate with a 0 RPM. Figure 6d shows a cross-sectional HRTEM image. The image clearly
20 displays the formation of a crystalline layer on top of the amorphous layer. The HRTEM image
21 indicates that colloidal ZnO nanocrystals formed in the helical reactor were first deposited on top
22 of the amorphous layer to form a layer of crystalline ZnO. The molecular and ionic precursors
23 were then served as the building units for the growth of ZnO NW arrays from the crystalline

1 ZnO seed layer. Dense, crystalline ZnO NWs with uniform length and diameter could be seen
2 from the SEM, HRTEM, FFT images and XRD pattern (Figure 6a-e). The SEM image of a
3 vertical NW array grew to an average height around 5.7 μm after a two-hour deposition period is
4 shown in Figure 6b. The aspect ratios of ZnO NWs can be controlled by varying the deposition
5 period and thickness of the amorphous layer.

6 We changed the flow rate of the chemical solution from 6.8 mL min^{-1} to 14.7 or 28.1 mL min^{-1}
7 and delivered the solution on the amorphous ZnO layer with a 0 RPM. Instead of growing
8 vertical ZnO NW arrays, continuous crystalline ZnO film with 347 nm thickness was obtained
9 after a three minute deposition period (Figure 6f-i). Figure 6f exhibits a polycrystalline film
10 consisting of densely packed ZnO grains, which is verified by convergent beam electron
11 diffraction patterns. The rectangular, spherical assemblies and individual ZnO nanocrystals
12 formed in the microchannel at these flow rates function as the seeds that lead to the growth of
13 densely packed crystalline ZnO film. The XRD pattern indicates a crystalline ZnO film with a
14 [001] preferred orientation (Figure 6i).

15 For comparison, we also performed the deposition using the same precursor concentration and
16 reaction temperature in a batch reactor. Loosely bound flower-like structures on the substrate,
17 which could be easily removed after rinsing with D.I. water, were collected after the batch
18 reaction (Figure 7). These observations suggest that the flower-like structures were formed via
19 homogeneous nucleation and growth in the solution rather than grown from the surface. This
20 comparison study clearly demonstrates that the ability to control the formation and transport of
21 ZnO nanocrystals, their assemblies, molecular and ionic precursors within the microreactor is
22 critical in achieving ZnO nanofilms with various morphologies. A summary of the synthesis,

1 assembly and deposition of ZnO nanofilms using the continuous flow microreactor system is
2 illustrated in Figure 8 and summarized in Table 1.

3 Photographs of the ZnO nanofilms were taken and are shown in Figure 9. The amorphous film
4 shows a highly reflective surface while the flower-like film has an opaque appearance and
5 exhibits gray color due to scattering of irregular flower structure. The vertical ZnO NW arrays is
6 translucent, and the crystalline film shows a certain color which depends on the thickness of the
7 film. The optical band gap of the nanofilm was measured after the thermal treatment at 500 °C
8 for one hour (Figure 10). The band gap of nanofilm was found to be identical, exhibiting about
9 3.3 eV regardless of the morphology of the nanofilm. The morphologies of the films were not
10 affected by the thermal treatment except for the amorphous thin film. After the thermal treatment,
11 the amorphous film possessed nano-pores (Figure 11).

12 Two-phase pool boiling experiments were performed using ZnO nanofilms on stainless steel
13 substrate as boiling surfaces to demonstrate the impact of different micro- and nanostructures of
14 these nanofilms. The morphologies of the ZnO thin films were found to be independent of the
15 substrate type, showing identical morphologies. This result supports that ZnO film morphologies
16 were controlled by the ZnO seed layer formed in-situ from the microreactor. Electronic system
17 energy management and cooling for future advanced lasers, radars, and power electronics are
18 getting more challenging, resulting in a search for technologies and design techniques to
19 dissipate ultra-high heat fluxes.³⁶ One promising approach to meet efficient heat dissipation is
20 utilizing the large latent heat of vaporization. Associated with the latent heat of vaporization,
21 wettability and surface geometry are the key parameters determining heat transfer
22 performances.^{25, 37-42} We conducted the pool boiling experiments with the ZnO nanofilms
23 including flower-like structures, vertical ZnO NW arrays, and crystalline film. The amorphous

1 thin film was not included for the experiments since nanopores have generally attenuated the
2 boiling performances.⁴³⁻⁴⁵ All of the ZnO nanofilms showed a reduced contact angle compared to
3 the bare surface, following the Wenzel's model as shown in Figure 12a.⁴⁶ The pool boiling
4 curves of the ZnO thin films were constructed by measuring super heat variation as a function of
5 given heat flux (Figure 12b). Critical heat flux (CHF) values of the nanofilms generally
6 increased as compared to the bare surface except for the vertical NW arrays. The highest CHF
7 value of around 100 W/cm^2 was obtained from crystalline film. The corresponding heat transfer
8 coefficient (HTC) of the nanofilms was calculated using Newton's law of cooling (Figure 12c).
9 As expected from the boiling curves, the crystalline film exhibited the highest HTC values of 4.2
10 $\text{W/cm}^2 \text{ K}$. The CHF value achieved from the crystalline film is about 20 percent improved
11 compared to one reported in our previous boiling experiment in reference [25].

12

13 CONCLUSIONS

14 ZnO nanofilms with four distinctly different morphologies were fabricated by adjusting
15 physical parameters including the flow rate of the solution and RPM of the rotating disk in the
16 continuous flow microreactor system while keeping the same chemical precursors, precursor
17 solution concentration, and reaction temperature. The morphology variation of the nanofilms
18 resulted from the controlled synthesis and transport of reactive species which were formed *in-*
19 *situ* in the helical microchannel reactor. The interactions between the Dean vortices and the
20 electrostatic repulsive force result in the formation of nanocrystal assemblies with different
21 morphologies. These assemblies serve as seed layers and play important roles in shaping the
22 morphologies of ZnO nanofilms. The pool boiling experiments clearly demonstrate the structural
23 impact of the nanofilms in the boiling heat transfer. This work demonstrates a highly-controlled

- 1 and scalable process that could be used to fabricate tailored metal oxide nanofilms for thin film
- 2 transistors, sensors, photocatalytic cells, solar cells, and two-phase heat exchangers.

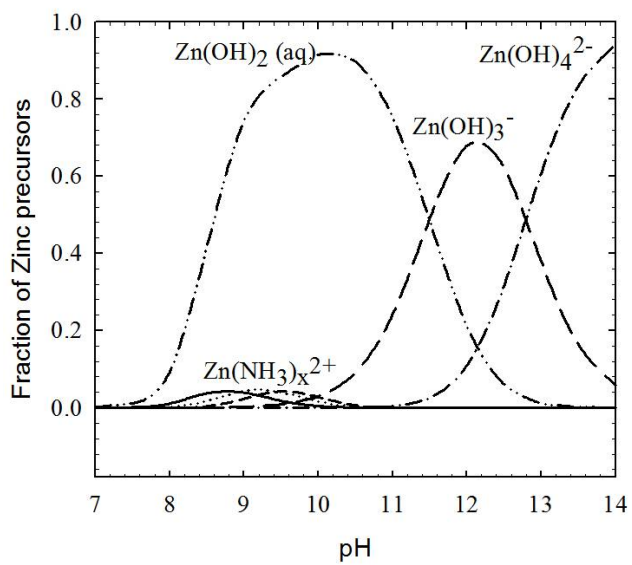


Figure 1. Speciation diagram of zinc precursors as a function of solution pH.

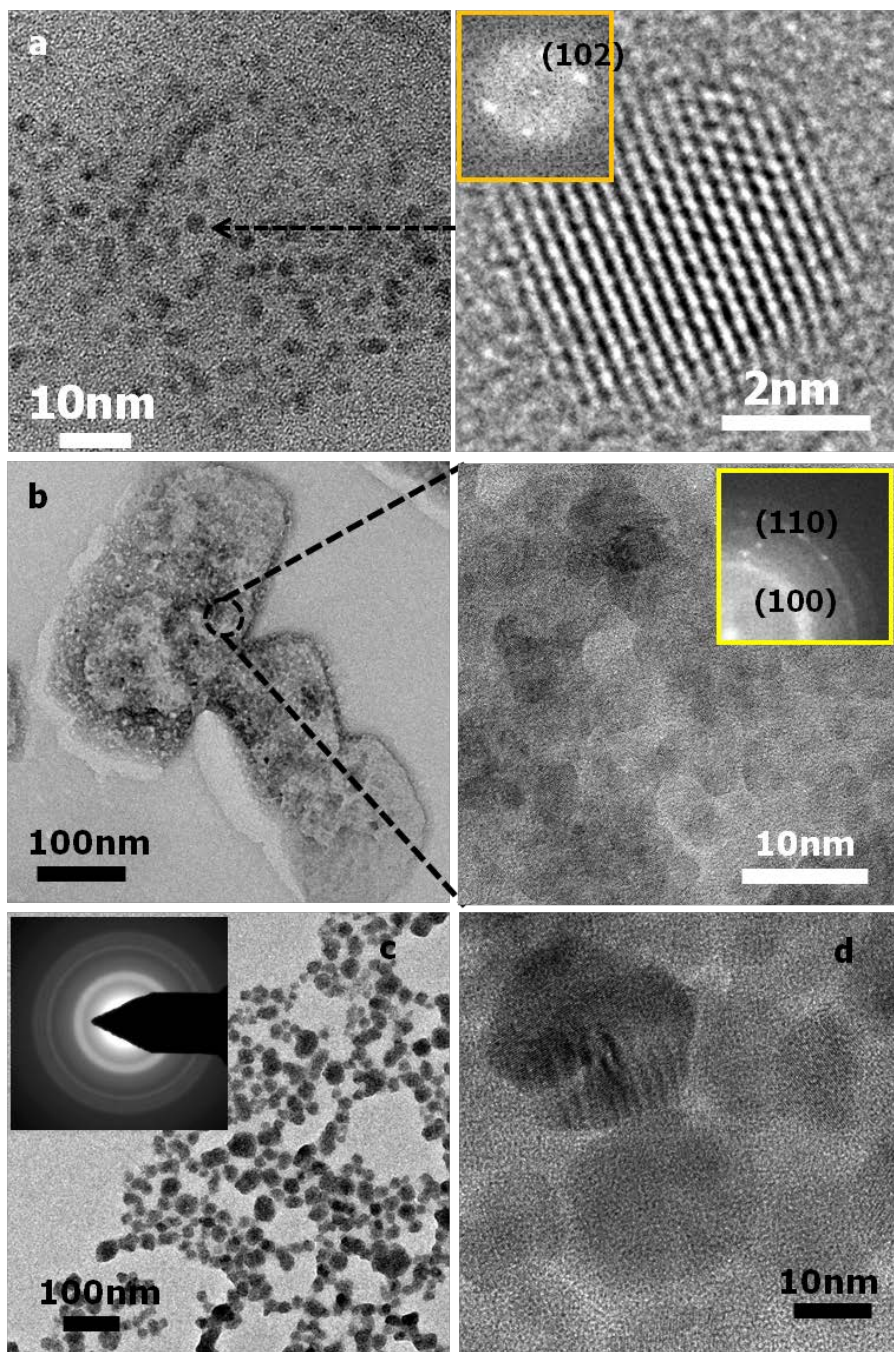


Figure 2. State of colloidal ZnO nanocrystals synthesized at various flow rates of solution: (a) individual nanocrystals at 6.8 mL min^{-1} , (b) rectangular assembly at 14.7 mL min^{-1} , (c) spherical assembly at 28.1 mL min^{-1} and selected area electron diffraction (SAED, inset) pattern, and (d) a close view of spherical assembly.

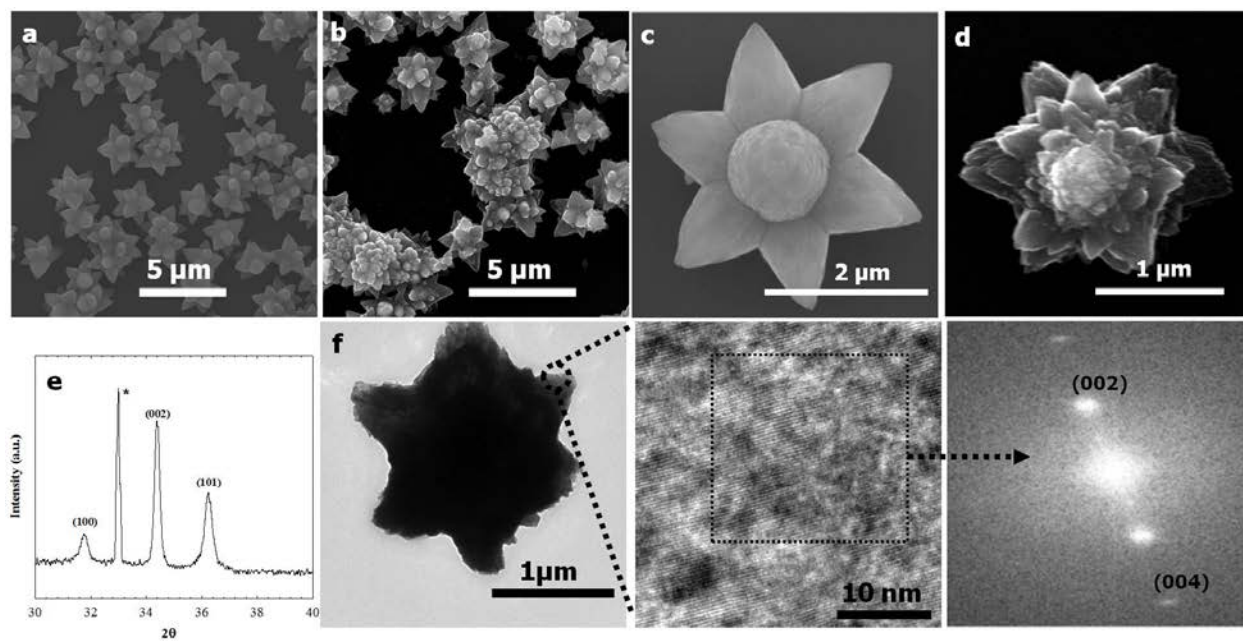


Figure 3. Flower-like film: Low and high magnification SEM image of film prepared from (a, c) 14.7 mL min^{-1} and (b, d) 28.1 mL min^{-1} flow rate, (e) XRD pattern (*: Si peak from SiO_2 substrate), (f) HRTEM and FFT image.

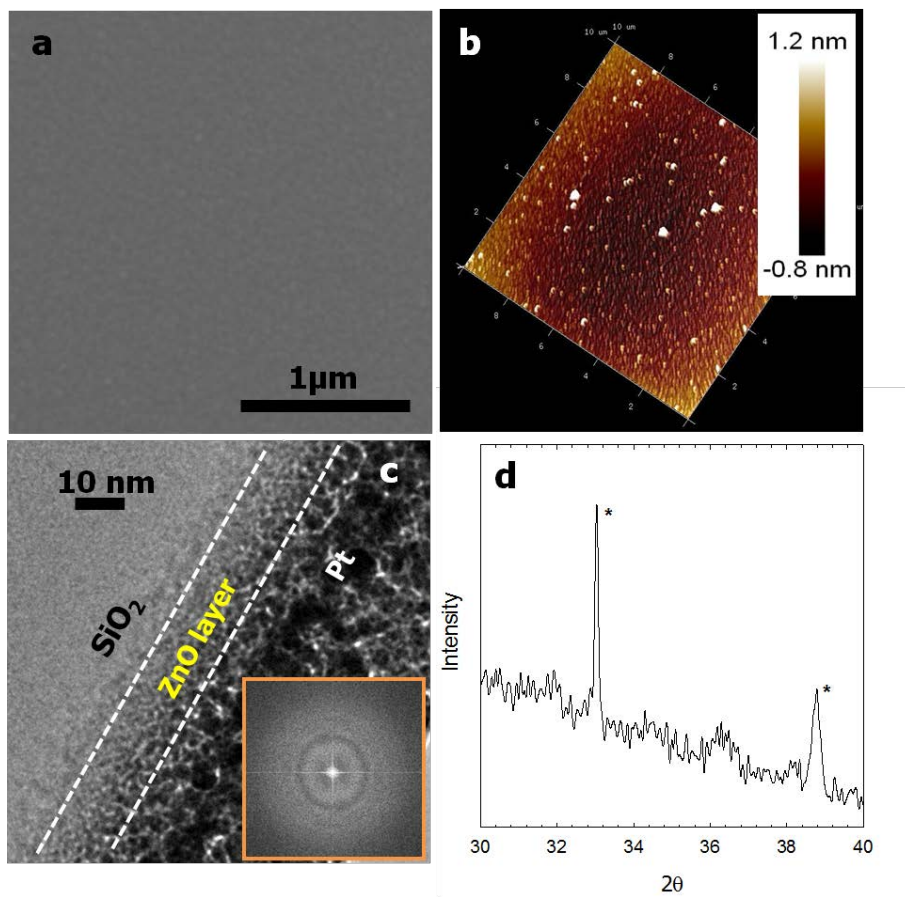


Figure 4. Amorphous thin film: (a) SEM image, (b) AFM image, (c) HRTEM image with FFT (inset), and (d) XRD pattern (*: Si peak from SiO₂ substrate).

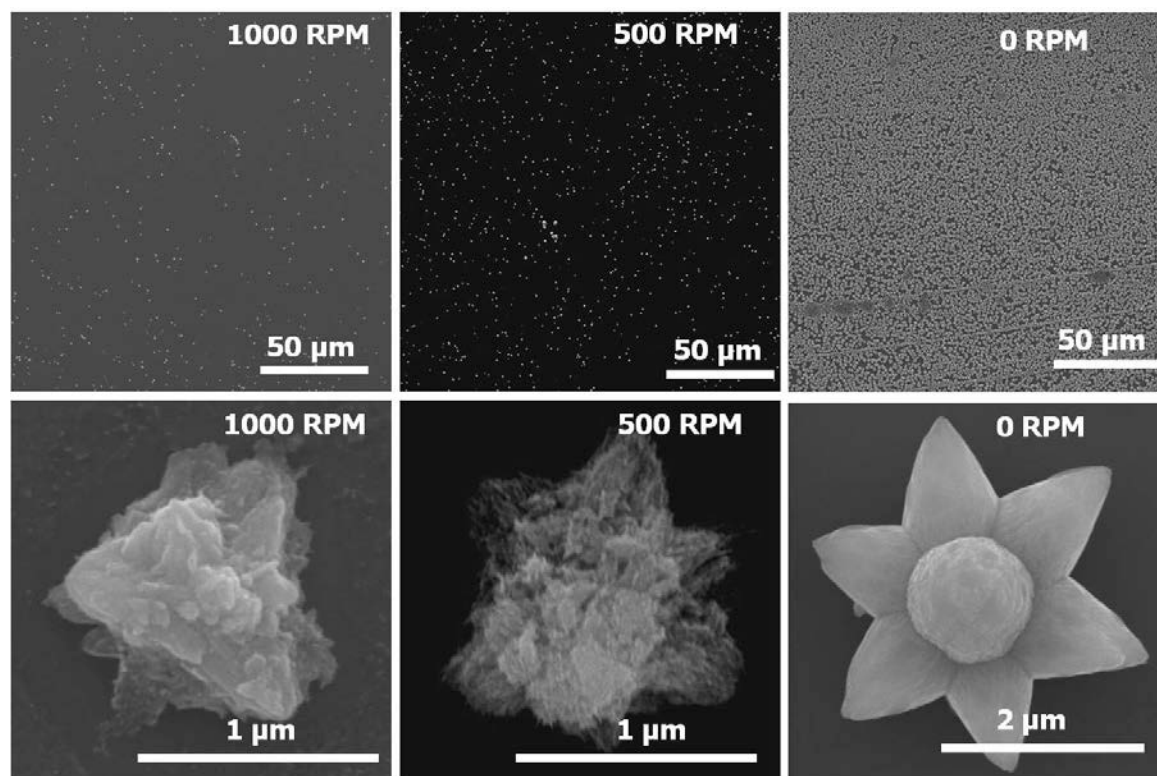


Figure 5. Low resolution (top) and high resolution (bottom) SEM images of flower-like films prepared at various RPM.

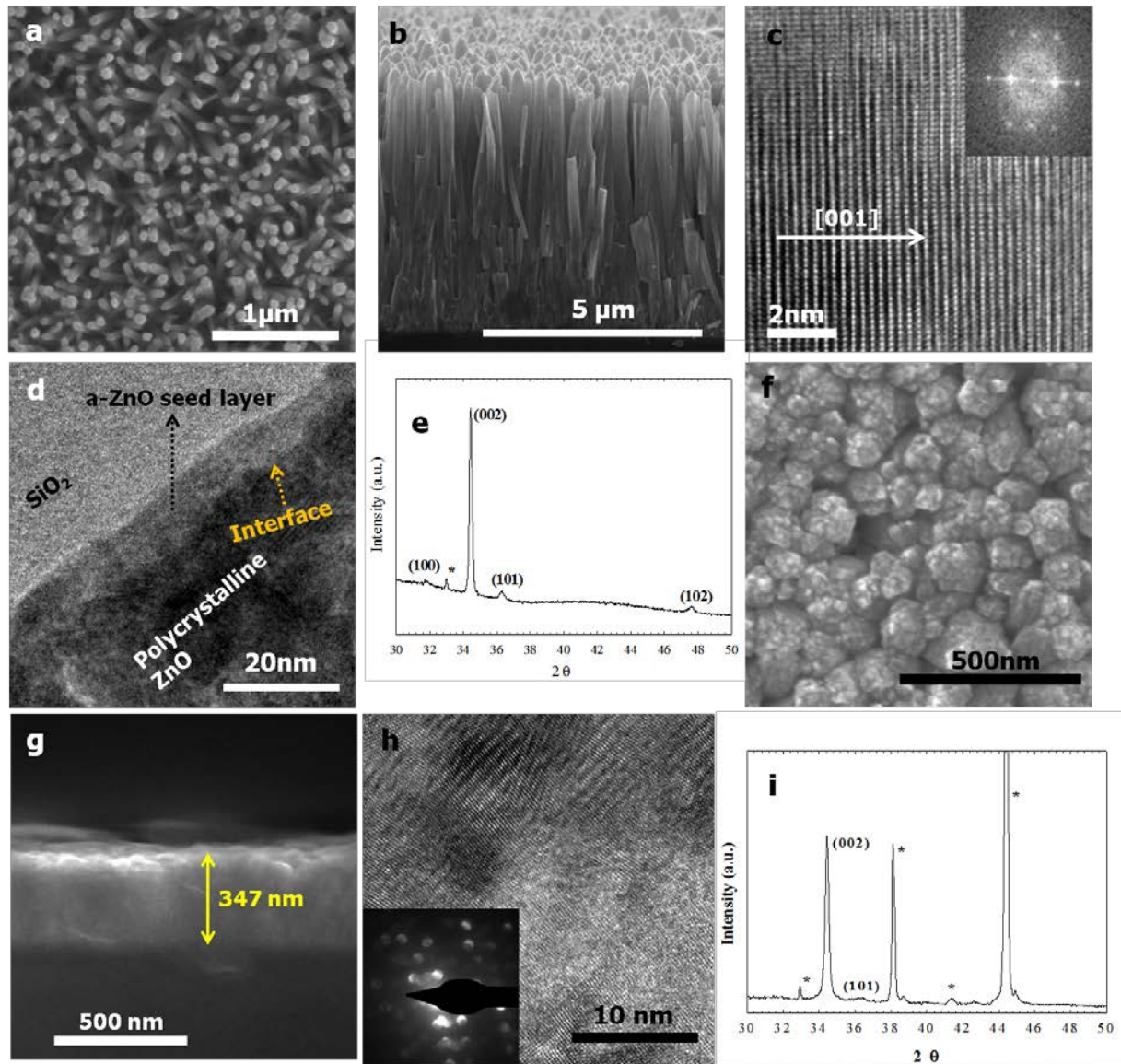


Figure 6. Vertical NW arrays: (a, b) Top and cross sectional SEM image, (c) HRTEM image and FFT (inset) of NW, (d) HRTEM image showing the interface between amorphous layer and polycrystalline layer (e) XRD pattern. Crystalline film: (f, g) Top and cross sectional SEM image, (h) HRTEM image with CBEM (inset), and (i) XRD pattern (*: Si peak from SiO₂ substrate).

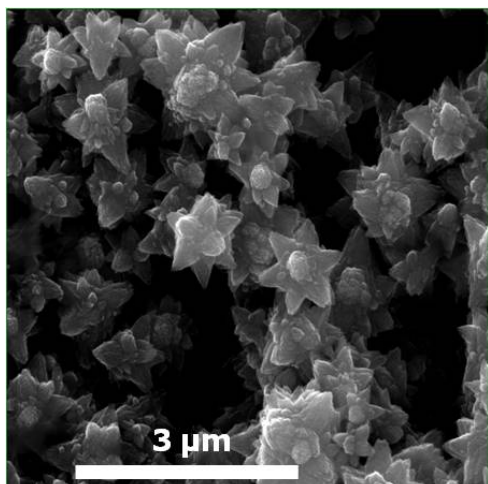


Figure 7. SEM image of powdery flower-like structure synthesized by a chemical bath process.

Table 1. Summary of process parameters and prepared ZnO nanofilms

Nanofilm	Flow rate (mL min ⁻¹)	Primary Reactive species	RPM	Reaction temp. (°C)	Substrate
Amorphous ZnO film (a- ZnO)	28.1	Zn(OH) ₃ ⁻	1500	70	SiO ₂ /Si
Flower like ZnO film	14.7 or 28.1	Seed: ZnO Assembly, Zn(OH) ₃ ⁻	0	70	SiO ₂ /Si
Vertical NW ZnO arrays	6.8	Seed: ZnO Nanocrystal, Zn(OH) ₃ ⁻	0	70	a-ZnO/SiO ₂ /Si
Crystalline ZnO film	14.7 or 28.1	Seed: ZnO Assembly, Zn(OH) ₃ ⁻	0	70	a-ZnO/SiO ₂ /Si

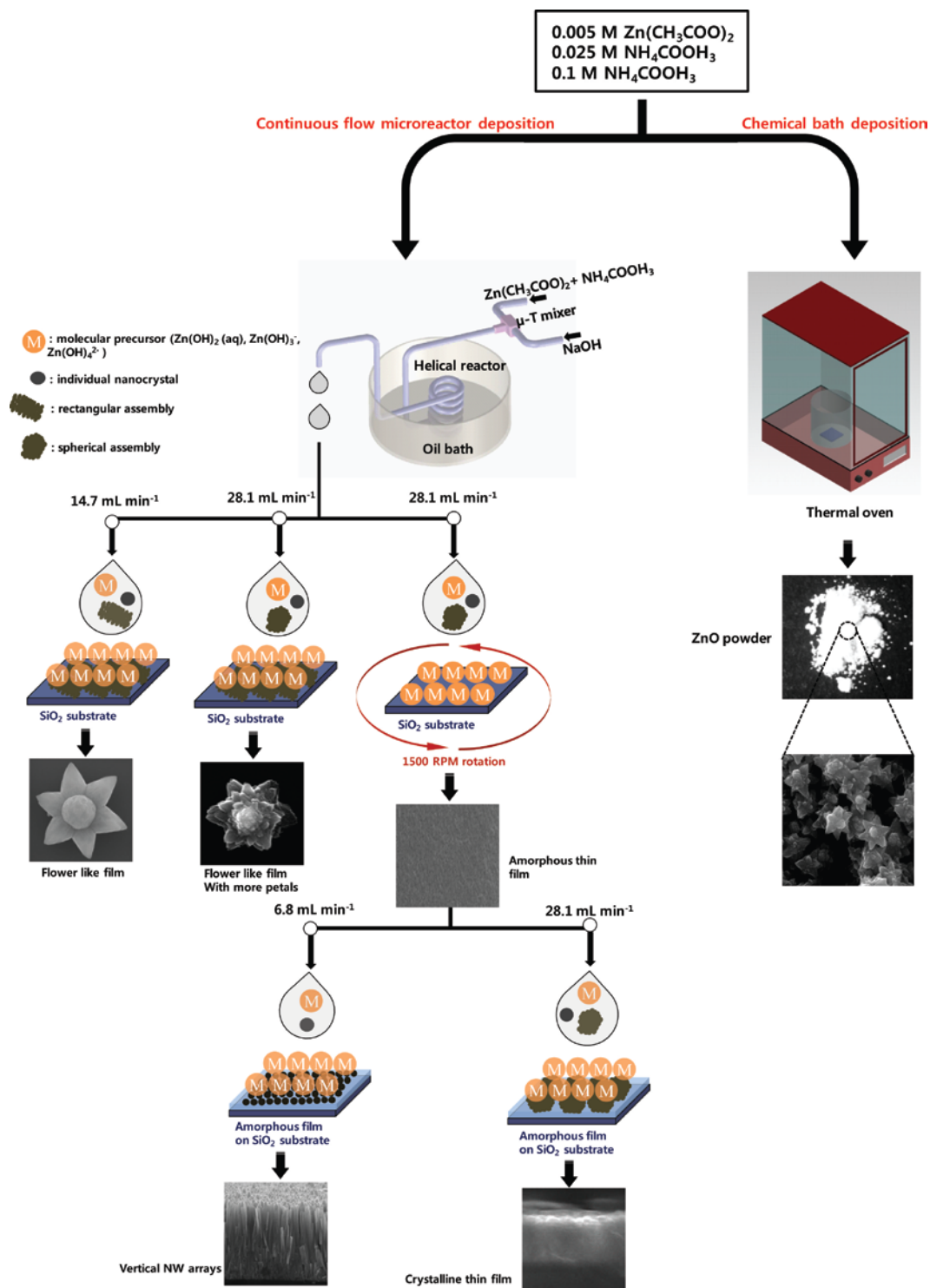


Figure 8. Illustrative comparison of ZnO nanofilms with various morphologies prepared by the continuous flow microreactor deposition with flower like structure prepared by a chemical bath deposition.

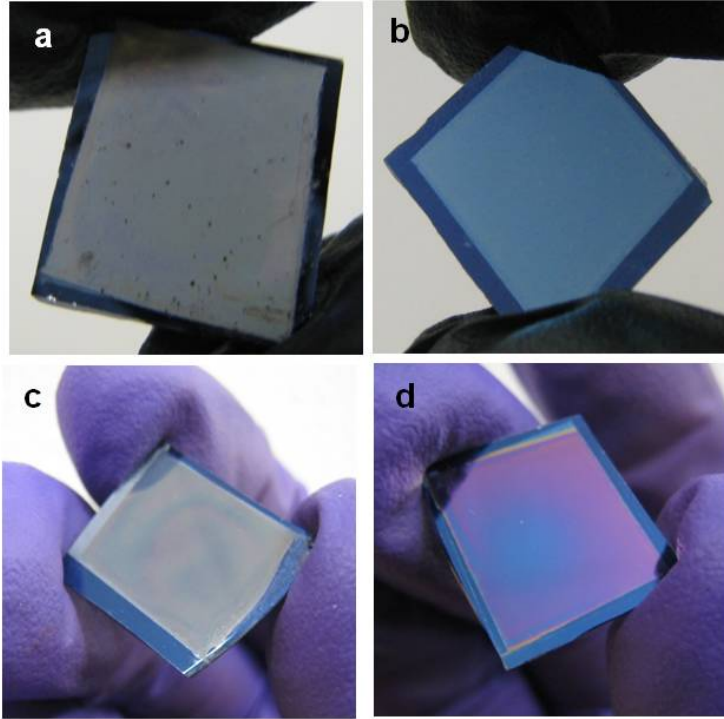


Figure 9. Photograph of ZnO nanofilms prepared on thermally grown oxide layer (100 nm) of Si substrate ($1.5\text{ cm} \times 1.5\text{ cm}$): (a) Flower like film with $1\mu\text{m}$ thickness, (b) amorphous film with 15 nm thickness, (c) vertical ZnO NW arrays with $5.7\mu\text{m}$ height, and (d) crystalline film with 347 nm thickness.

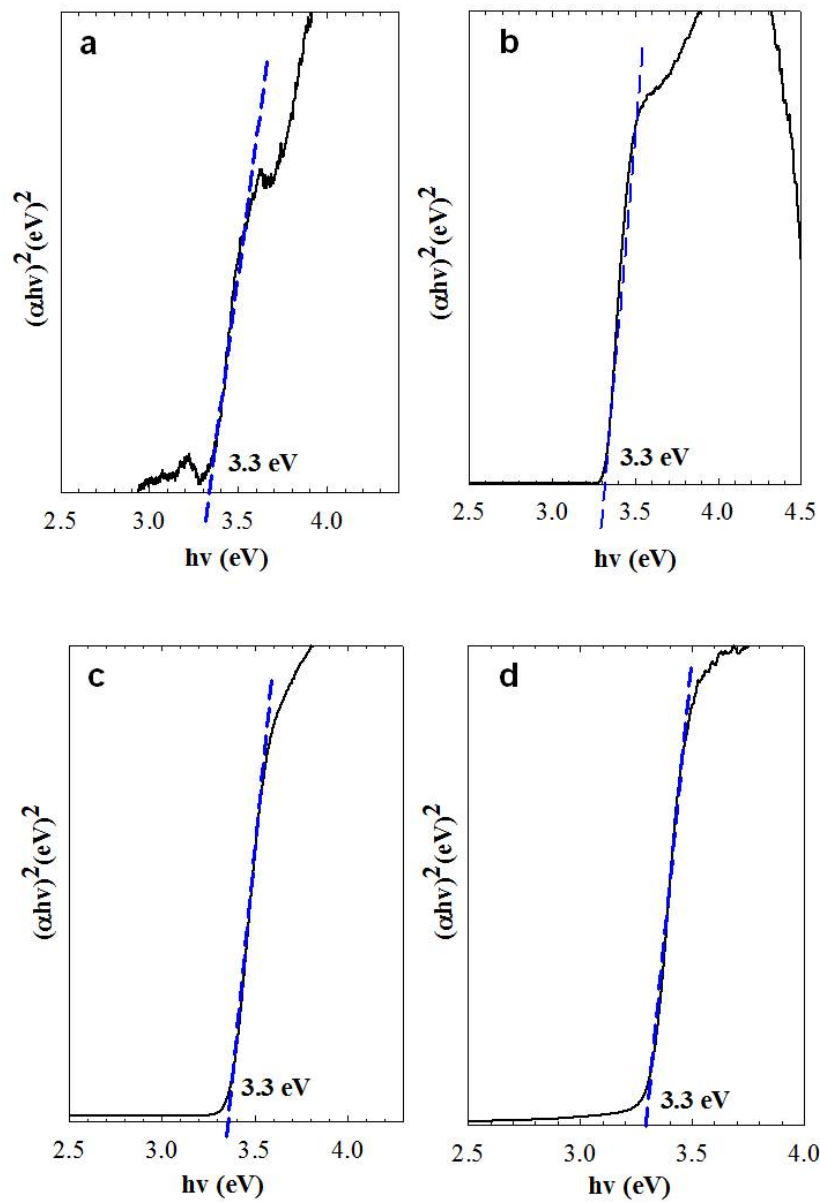


Figure 10. Optical band gap of ZnO nanofilms: (a) Flower like film, (b) amorphous film, (c) vertical NW arrays, and (d) crystalline film.

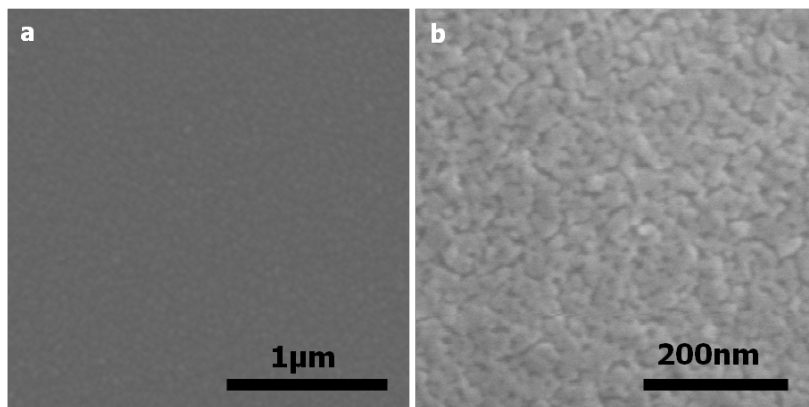


Figure 11. SEM images of amorphous ZnO films: (a) as-deposited film and (b) after thermal annealing at 500 °C for one hour.

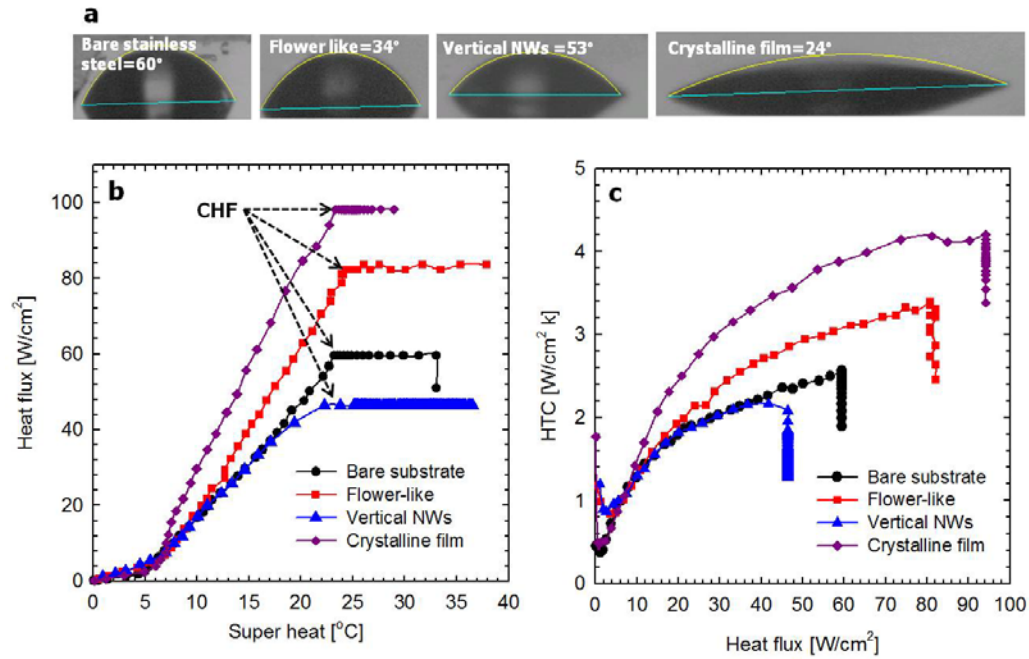


Figure 12. Pool boiling experiments: (a) Contact angle measurement of the nanofilms, (b) pool boiling curve, (c) heat transfer coefficient curve as a function of heat flux.

ASSOCIATED CONTENT

Supporting Information

AUTHOR INFORMATION

Corresponding Author

* E-mail: chih-hung.chang@oregonstate.edu

ACKNOWLEDGMENT

This work was performed in the Oregon Process Innovation Center (OPIC) within the Microproduct Breakthrough Institute (MBI) supported by Oregon Built Environment & Sustainable Technologies (Oregon BEST) and the Oregon Nanoscience and Micro-technologies Institute (ONAMI). Katherine Han's assistance in editing this paper is highly appreciated. Funding was provided by US Army Communications-Electronics Research, Development, and Engineering Center (CERDEC) through the Tactical Energy System program W909MY-10-C-0073, Sharp Laboratories of America Scholar Fund and National Science Foundation Process and Reaction Engineering Program under grant number CBET-1105061. National Science Foundation via the Major Research Instrumentation (MRI) Program under Grant No. 1040588.

REFERENCES

- (1) Granqvist, C. G. *Sol. Energy Mater. Sol. Cells* **2012**, *99*, 166-175.
- (2) Li, Y.; Yang, X.-Y.; Feng, Y.; Yuan, Z.-Y.; Su, B.-L. *Crit. Rev. Solid State Mater. Sci.* **2012**, *37*, 1-74.
- (3) Osterloh, F. E. *Chem. Soc. Rev.* **2013**, *42*, 2294-2320.
- (4) Ozgur, U.; Alivov, Y. I.; Liu, C.; Teke, A.; Reshchikov, M. A.; Dogan, S.; Avrutin, V.; Cho, S. J.; Morkoc, H. *J. Appl. Phys.* **2005**, *98*, 041301.
- (5) Huang, M. H.; Mao, S.; Feick, H.; Yan, H. Q.; Wu, Y. Y.; Kind, H.; Weber, E.; Russo, R.; Yang, P. D. *Science* **2001**, *292*, 1897-1899.
- (6) Xu, S.; Qin, Y.; Xu, C.; Wei, Y.; Yang, R.; Wang, Z. L. *Nat. Nanotechnol.* **2010**, *5*, 366-373.
- (7) Law, M.; Greene, L. E.; Johnson, J. C.; Saykally, R.; Yang, P. D. *Nat. Mater.* **2005**, *4*, 455-459.
- (8) Han, S.-Y.; Paul, B. K.; Chang, C.-h. *J. Mater. Chem.* **2012**, *22*, 22906-22912.
- (9) Baxter, J. B.; Aydil, E. S. *J. Electrochem. Soc.* **2009**, *156*, H52-H58.
- (10) Yang, P. D.; Yan, H. Q.; Mao, S.; Russo, R.; Johnson, J.; Saykally, R.; Morris, N.; Pham, J.; He, R. R.; Choi, H. J. *Adv. Funct. Mater.* **2002**, *12*, 323-331.
- (11) Govender, K.; Boyle, D. S.; Kenway, P. B.; O'Brien, P. J. *J. Mater. Chem.* **2004**, *14*, 2575-2591.

- (12) Sounart, T. L.; Liu, J.; Voigt, J. A.; Huo, M.; Spoerke, E. D.; McKenzie, B. *J. Am. Chem. Soc.* **2007**, *129*, 15786-15793.
- (13) Kaluza, S.; Schroeter, M. K.; d'Alnoncourt, R. N.; Reinecke, T.; Muhler, M. *Adv. Funct. Mater.* **2008**, *18*, 3670-3677.
- (14) Tian, Z. R. R.; Voigt, J. A.; Liu, J.; McKenzie, B.; McDermott, M. J.; Rodriguez, M. A.; Konishi, H.; Xu, H. F. *Nat. Mater.* **2003**, *2*, 821-826.
- (15) Wang, X.; Liao, M.; Zhong, Y.; Zheng, J. Y.; Tian, W.; Zhai, T.; Zhi, C.; Ma, Y.; Yao, J.; Bando, Y.; Golberg, D. *Adv. Mater.* **2012**, *24*, 3421-3425.
- (16) Han, S. Y.; Chang, Y. J.; Lee, D. H.; Ryu, S. O.; Lee, T. J.; Chang, C. H. *Electrochem. Solid-State Lett.* **2007**, *10*, K1-K5.
- (17) Jung, J. Y.; Park, N.-K.; Han, S.-Y.; Han, G. B.; Lee, T. J.; Ryu, S. O.; Chang, C.-H. *Current Applied Physics* **2008**, *8*, 720-724.
- (18) Li, S.; Gross, G. A.; Guenther, P. M.; Koehler, J. M. *Chem. Eng. J.* **2011**, *167*, 681-687.
- (19) McPeak, K. M.; Baxter, J. B. *Cryst. Growth Des.* **2009**, *9*, 4538-4545.
- (20) McPeak, K. M.; Baxter, J. B. *Ind. Eng. Chem. Res.* **2009**, *48*, 5954-5961.
- (21) Han, S.-Y.; Paul, B. K.; Chang, C.-h. *J. Mat. Chem.* **2012**, *22*, 22906-22912.
- (22) Kim, S.; Lee, S. J. *Exp. Fluids* **2009**, *46*, 255-264.
- (23) Choi, C.-H.; Su, Y.-W.; Chang, C.-h. *CrystEngComm* **2013**, *15*, 3326-3333.

- (24) Tan, S. T.; Chen, B. J.; Sun, X. W.; Fan, W. J.; Kwok, H. S.; Zhang, X. H.; Chua, S. J. *J. Appl. Phys.* **2005**, *98*, 013505.
- (25) Hendricks, T. J.; Krishnan, S.; Choi, C.; Chang, C.-H.; Paul, B. *Int. J. Heat Mass Transfer* **2010**, *53*, 3357-3365.
- (26) McBride, R. A.; Kelly, J. M.; McCormack, D. E. *J. Mater. Chem.* **2003**, *13*, 1196-1201.
- (27) Lee, S.; Bae, S.-H.; Lin, L.; Yang, Y.; Park, C.; Kim, S.-W.; Cha, S. N.; Kim, H.; Park, Y. J.; Wang, Z. L. *Adv. Funct. Mater.* **2013**, *23*, 2445-2449.
- (28) Bai, Y.; Yu, H.; Li, Z.; Amal, R.; Lu, G. Q.; Wang, L. *Adv. Mater.* **2012**, *24*, 5850-5856.
- (29) Zhang, Y.; Yan, X.; Yang, Y.; Huang, Y.; Liao, Q.; Qi, J. *Adv. Mater.* **2012**, *24*, 4647-4655.
- (30) Lee, J.; Cha, S.; Kim, J.; Nam, H.; Lee, S.; Ko, W.; Wang, K. L.; Park, J.; Hong, J. *Adv. Mater.* **2011**, *23*, 4183.
- (31) Lee, Y. T.; Jeon, P. J.; Lee, K. H.; Ha, R.; Choi, H.-J.; Im, S. *Adv. Mater.* **2012**, *24*, 3020-3025.
- (32) Greene, L. E.; Law, M.; Tan, D. H.; Montano, M.; Goldberger, J.; Somorjai, G.; Yang, P. *D. Nano Lett.* **2005**, *5*, 1231-1236.
- (33) Song, J.; Lim, S. *J. Phys. Chem. C* **2007**, *111*, 596-600.
- (34) Vayssieres, L. *Adv. Mater.* **2003**, *15*, 464-466.

- (35) Fan, H. J.; Lee, W.; Scholz, R.; Dadgar, A.; Krost, A.; Nielsch, K.; Zacharias, M. *Nanotechnology* **2005**, *16*, 913-917.
- (36) Mudawar, I. *IEEE Trans. on Compon. Packag. Technol.* **2001**, *24*, 122-141.
- (37) Rainey, K. N.; You, S. M. *J. Heat Transfer* **2000**, *122*, 509-516.
- (38) Arik, M.; Bar-Cohen, A.; You, S. M. *Int. J. Heat Mass Transfer* **2007**, *50*, 997-1009.
- (39) Xu, J.; Ji, X.; Zhang, W.; Liu, G. *Int. J. Multiphase Flow* **2008**, *34*, 1008-1022.
- (40) Jo, H.; Kim, S.; Kim, H.; Kim, J.; Kim, M. H. *Nanoscale Res. Lett.* **2012**, *7*, 242.
- (41) Chu, K.-H.; Joung, Y. S.; Enright, R.; Buie, C. R.; Wang, E. N. *Appl. Phys. Lett.* **2013**, *102*, 151602.
- (42) O'Hanley, H.; Coyle, C.; Buongiorno, J.; McKrell, T.; Hu, L.-W.; Rubner, M.; Cohen, R. *Appl. Phys. Lett.* **2013**, *103*, 024102.
- (43) Chen, R.; Lu, M.-C.; Srinivasan, V.; Wang, Z.; Cho, H. H.; Majumdar, A. *Nano Lett.* **2009**, *9*, 548-553.
- (44) Chen, J.; Wiley, B. J.; Xia, Y. *Langmuir* **2007**, *23*, 4120-4129.
- (45) Tong, L. S.; Tang, Y. S., *Boiling Heat Transfer and Two Phase Flow*. In ed.; Taylor & Francis: London, 1997.
- (46) Patankar, N. A. *Langmuir* **2010**, *26*, 8941-8945.

SYNOPSIS

We employ a continuous flow microreactor and deposition system to fabricate ZnO nanofilms with various morphologies including flower-like structure, amorphous film, vertical NW arrays, and crystalline film. In contrast, only powdery flower-like ZnO could be obtained using a batch reactor. This study demonstrates the versatility of a continuous flow microreactor and deposition for the nanostructures production with various morphologies by tuning the physical process parameters while using the same chemical precursors, concentration, and reaction temperature.

TABLE OF CONTENTS

